Atmos. Chem. Phys. Discuss., 15, 17527–17552, 2015
www.atmos-chem-phys-discuss.net/15/17527/2015/
doi:10.5194/acpd-15-17527-2015

Atmospheric Chemistry and Physics Discussions

Effect of retreating sea ice on Arctic cloud cover in simulated recent global warming

M. Abe[1], T. Nozawa[2], T. Ogura[3], and K. Takata[4,3,1]

[1]Japan Agency for Marine-Earth Science and Technology, Yokohama, Japan
[2]Okayama University, Okayama, Japan
[3]National Institute for Environmental Studies, Tsukuba, Japan
[4]National Institute of Polar Research, Tachikawa, Japan

Received: 05 June 2015 – Accepted: 10 June 2015 – Published: 30 June 2015

Correspondence to: M. Abe (abe.mnb@gmail.com)

Published by Copernicus Publications on behalf of the European Geosciences Union.

Abstract

This study investigates the effect of sea ice reduction on Arctic cloud cover in historical simulations with the coupled atmosphere–ocean general circulation model MIROC5. During simulated global warming since the 1970s, the Arctic sea ice extent has reduced substantially, particularly in September. This simulated reduction is consistent with satellite observation results. However, the Arctic cloud cover increases significantly during October at grids with significant reductions in sea ice because of the enhanced heat and moisture flux from the underlying ocean. Cloud fraction increases in the lower troposphere. However, the cloud fraction in the surface thin layers just above the ocean decreases despite the increased moisture because the surface air temperature rises strikingly in the thin layers and the relative humidity decreases. As the cloud cover increases, the cloud radiative effect in surface downward longwave radiation (DLR) increases by approximately 40–60 % compared to a change in clear-sky surface DLR. These results suggest that an increase in the Arctic cloud cover as a result of a reduction in sea ice could further melt the sea ice and enhance the feedback processes of the Arctic amplification in future projections.

1 Introduction

Satellite observations have shown that the Arctic sea ice extent has reduced gradually since the 1980s (Comiso et al., 2008). Recent significant reductions in the Arctic sea ice occurred in 2007 and 2012. A further reduction in Arctic sea ice is likely to result from global warming. In turn, the reduction in sea ice can accelerate surface warming in the Arctic region and at a global scale through various feedback processes. A major feedback process in climate change is the ice-albedo feedback, in which the reduced sea ice extent decreases the global albedo and then increases shortwave radiation entering into the climate system (e.g., Curry et al., 1995; Dickinson et al., 1987; Manabe and Stouffer, 1980; Perovich et al., 2007). This feedback is likely to occur in high-

ACPD
15, 17527–17552, 2015

latitude regions, where snow cover and sea ice are seasonally extended. Thus, the ice-albedo feedback is more dominant in the autumn, when the incoming shortwave radiation is not at its lowest values in the high-latitude region (Yoshimori et al., 2014).

However, the reduction in sea ice involves other feedback processes in the Arctic region (Serreze and Barry, 2011). Previous studies suggest that extended periods open ocean resulting from reductions in sea ice increased the Arctic cloud cover and enhanced the Arctic amplification (AA) (e.g., Holland and Bitz, 2003; Screen and Simmonds, 2010; Serreze and Barry, 2011; Vavrus et al., 2009). With regard to recent changes in the Arctic cloud cover, Schweiger (2004) reported that both satellite data from TIROS Operational Vertical Sounder (TOVS) Polar Pathfinder retrievals and Advanced Very High Resolution Radiometer (AVHRR) data revealed significant decreases in cloud fractions over the Arctic sea during winter (December–January–February, DJF) and striking increases in spring (March–April–May, MAM) cloudiness. Wang and Key (2003) also showed an increase in the spring cloud fraction. However, the negative trend in spring cloudiness reported by Comiso (2003) is not consistent with these previous findings. These results suggest that uncertainty remains with respect to these observations. Therefore, continuous monitoring and investigation of the changes in Arctic cloudiness are required for a robust evaluation.

To monitor the change in cloudiness resulting from reduced sea ice, several recent studies have used satellite data. Liu et al. (2012) evaluated the use of satellite data to show that a 1 % decrease in sea ice concentration leads to a 0.36–0.47 % increase in cloud cover. These authors also suggested that the total variance in the cloud cover from July to November can be explained by sea ice-cloud feedback. Using satellite data, Wu and Lee (2012) showed that the autumn low cloud cover over the Beaufort Sea and East Siberian Sea increased during 2000–2010, notably in October. The authors suggested that the enhanced downward longwave radiation (DLR) resulting from the increased cloud cover may be responsible for the enhanced autumnal warming in surface air temperature (SAT). In addition, the enhanced DLR can prolong the sea ice melt seasons and lead to a positive feedback involving Arctic sea ice loss.

ACPD
15, 17527–17552, 2015

Furthermore, a strong link between cloud cover variability and sea ice variability near the sea ice margins was found in autumn using the 40 year ECMWF Re-Analysis (ERA40) data and TOVS polar Pathfinder satellite datasets (Schweiger et al., 2008). However, this previous study concluded that the radiative effect of this change is relatively small because the direct radiative effects of the cloud cover changes are compensated for by changes in the temperature and humidity profiles associated with varying ice conditions. A regional climate model simulation has also shown that the radiative effect of the changes in cloud cover is likely to be smaller than that of changes in air temperature and humidity (Rinke et al., 2013). Because of the deficiency of observed radiation data at the surface, correctly evaluating the radiative effect of the cloud cover change is difficult. Therefore, the radiative effect of cloud clover changes in the AA is controversial.

Recent ship observations found that the cloud base height in September tends to increase over the Arctic ocean without sea ice cover because of heating from the ocean. This heating is enhanced because of the increased temperature gradient between the atmosphere and the ocean, weakening the stable conditions in the atmospheric boundary layer (Sato et al., 2012). This previous study indicated that convective clouds increase in the Arctic Ocean. However, inconsistent results have been reported concerning the vertical profile of cloud cover change. Whereas Kay and Gettelman (2009) showed that increased turbulent transport of heat and moisture promotes low-cloud formations, Schweiger et al. (2008) showed that low-level clouds may decrease and simultaneously middle-level clouds may increase because the decreased static stability and a deepening atmospheric boundary layer contribute to a rise in the cloud level. Simulations run by Porter et al. (2012) with the Weather Research Forecasting (WRF) model support an increase in middle-level clouds in September and increases in low-level clouds from October to November. The vertical profile of the cloud cover change resulting from sea ice loss is under debate and may alter the evaluation of the radiative effect of cloud cover change.

ACPD
15, 17527–17552, 2015

In addition to the results from the observed data, several studies employ climate model simulations. Climate models that have simulated sea ice reduction show that the Arctic cloud cover increases in the autumn (Vavrus et al., 2011, 2009). An increased area of open ocean enhances the heat and moisture transport from the ocean to the atmosphere, resulting in an increased cloudiness. These studies analyzed the change in cloudiness resulting from sea ice losses in simulations with increasing greenhouse gas concentrations. The effects of reduced sea ice in these analyses are stronger than those occurring in the late 20th century. Therefore, these results are not always appropriate for the change in Arctic cloudiness occurring in the late 20th century and the present situation, in which the sea ice reduces only in limited regions. These investigations may be insufficient to understand the events observed recently and unable to effectively explain recent processes in simulated climate models.

As noted above, studies have investigated the Arctic cloud cover change during recent global warming. However, a debate remains surrounding the change in Arctic cloudiness and the lack of understanding of the effect of the reduced sea ice on Arctic cloud cover because of insufficient observed data. In addition, the radiative effect of the cloud cover change at the surface is difficult to measure accurately because of the dark seasons and sea ice cover. In this study, we investigate the temporal trends of Arctic cloud cover change during the recent global warming using a climate model simulation and focus on the effects of reduced sea ice. The vertical structure of the cloud cover change is analyzed using the composite analysis technique. Furthermore, changes in the cloud radiative effect in the surface DLR are evaluated to provide information on the role of Arctic clouds in the mechanism of the AA. The change in Arctic cloud resulting from the reduced sea ice in climate model simulations should be informative for understanding the mechanism underlying future changes in Arctic clouds and the AA.

The next section explains the coupled atmosphere–ocean general circulation model, MIROC5, used in this study and its 20th century simulation. The third section reports the results for the Arctic cloud cover change resulting from the retreating sea ice.

ACPD
15, 17527–17552, 2015

We then discuss the relationship between changes in Arctic cloud cover and sea ice change, and the paper concludes with a summary.

2 Model and experiments

We analyze historical simulations using a coupled atmosphere–ocean general circulation model, MIROC5 (Watanabe et al., 2010), a model that was used in the Coupled Model Intercomparison Project Phase 5 (CMIP5). The atmospheric portion of MIROC5 is based on the global spectral dynamical core and includes a standard physical package. The atmospheric resolution is T85L40, with the peak at 3 hPa. The ocean general circulation model in MIROC5 is the CCSR (Center for Climate System Research, University of Tokyo) Ocean Component Model (COCO) version 4.5 (Hasumi, 2007). The zonal resolution of the ocean is fixed at 1.4°, whereas the meridional resolution is 0.5° at latitudes equatorward of 8° and 1.4° at higher latitudes (poleward of 65°), with a smooth transition in between (256 × 224 grid points for zonal and meridional resolutions). The model has 49 vertical levels, and the spacing varies with a depth of 2.5 m at the surface, 20 m at a depth of 100, 100 m at a depth of 1000 m, and 250 m below the 2000 m depth. The sea ice in each horizontal grid is divided into five categories in addition to open water. The sea ice concentration, ice thickness, and energy of ice melting are predicted for the five categories in a grid cell (Komuro et al., 2012). The lower bounds of the ice thickness for these categories are 0.3, 0.6, 1.0, 2.5, and 5.0 m.

The historical simulations from 1850 to 2005 were performed using anthropogenic forcings recommended by the CMIP5 project. The historical change in the solar constant is considered according to Lean et al. (2005). The historical changes in the optical thickness of volcanic stratospheric aerosols are given by Sato et al. (1993), and subsequent updates are available (http://data.giss.nasa.gov/modelforce/strataer/index.html). Beginning in 1998, the optical thickness of the volcanic stratospheric aerosols exponentially reduced with a one-year relaxation time.

ACPD
15, 17527–17552, 2015

The historical simulation by MIROC5 has five ensemble members with different initial conditions. In this study, monthly mean data are used, and sea ice concentration data were interpolated to be in the identical horizontal grids as the atmosphere.

3 Results

3.1 Temporal trend of the Arctic sea ice and clouds

Figure 1a shows the time series of SAT anomalies (Δ SAT) from the 1951–1980 average, which are averaged for the global and the high-latitude regions (60–90° N) during 1900–2005. Before 1970, the global mean Δ SAT varied between −0.5 and 0.5 °C at an inter-annual variation scale. However, a small increasing trend occurred during 1900–1960 in the global mean Δ SAT; the interannual variations of the global mean Δ SAT are dominant. Since the 1970s, however, the global mean Δ SAT has increased with interannual variations. The warming rate of the global mean Δ SAT is approximately 0.2 K decade^{-1}. However, the Δ SAT (60–90° N) has also varied between −1.0 and +1.0 °C until 1970. The Δ SAT (60–90° N) started to increase in the 1970s, reaching 1 °C in the 2000s. The warming rate from 1976 to 2005 was approximately 0.6 K decade^{-1}, which is twice as high or higher than the warming rate for the global mean Δ SAT. This result clearly reveals the AA and demonstrates that the MIROC5 is able to simulate the AA in historical simulations. The positive trend for the Δ SAT (60–90° N) for 1970–2005 in MIROC5 is similar to that of the observation-based Δ SAT (60–90° N) data from the Merged Land and Ocean Temperature Analysis (MLOST) (Smith et al., 2008), HadCRUT4 (Morice et al., 2012) and GISS Surface Temperature Analysis (GISTEMP) (Hansen et al., 2010).

Figure 1b shows the time series of the September Arctic sea ice area. As the SAT in the northern high latitude increases, the Arctic sea ice area significantly decreases. This decrease from the 1970s is common in all ensemble members. The ensemble average of the September sea ice area is approximately 5.25×10^{-6} km^2 in 2005. This

ACPD
15, 17527–17552, 2015

simulated negative trend in the Arctic sea ice area is consistent with that from the Hadley Center Sea Ice and Sea Surface Temperature data set (HadISST) (Rayner et al., 2003) (Fig. 1b), although the simulated area is slightly larger than that from the HadISST.

Figure 2a shows the seasonal cycle of the Arctic sea ice area averaged for 1976–1985 (blue line) and 1991–2005 (red line), and Fig. 2b displays the differences in the seasonal cycle. The maximum sea ice area occurs in March, and the sea ice then decreases to reach a minimum in August. This seasonal cycle of sea ice area in the MIROC5 is slightly different from the observed seasonal cycle (Komuro et al., 2012). According to the observations, the seasonal minimum sea ice area occurs in September, and generally, the Arctic sea ice cover starts to recover in October. Although such discrepancies are found, the basic features of the seasonal cycle of the Arctic sea ice such as the summer reduction and autumn recovery in sea ice are simulated in the MIROC5. During recent global warming, the simulated Arctic sea ice decreased in all months from 1976 to 2005, displaying a maximum reduction in September. The maximum reduction in the Arctic sea ice area in September is consistent with the observations of the Arctic sea ice (Comiso et al., 2008).

For the cloud cover over the Arctic Ocean, Fig. 2c and d are identical to Fig. 2a and b except for the total and low-level cloud cover, respectively. The Arctic Ocean is covered by low-level clouds during the summer. From summer to autumn, the cloud cover over the Arctic Ocean decreases, reaching a minimum during April. The seasonal cycle of the total cloud cover is similar to that of the low-level clouds. Therefore, the seasonal cycle of the total cloud cover is able to be explained by that of the low-level clouds. When compared with the seasonal cycle of cloud cover observed by TOVS satellite and surface-based cloud climatology reported by Schweiger et al. (1999) and Hahn et al. (1995), the seasonal cycle of the total cloud cover averaged over the Arctic Ocean is realistically simulated using this method. As shown in Fig. 2d, the Arctic cloud cover for autumn-winter-spring increases during (1976–85)–(1996–2005) but not substantially. The increase in cloud cover is the largest in October. The increase in

ACPD
15, 17527–17552, 2015

the total cloud cover is also explained by the increase in low-level clouds. This result agrees with previous studies using satellite data and climate model simulations (Liu et al., 2012; Vavrus et al., 2011; Wu and Lee, 2012). Compared to the low-level cloud cover, the middle- and high-level cloud covers are small, and their changes during (1976–85)–(1996–2005) are approximately zero (not shown).

Figure 3 shows the geographical distributions of the linear trends in the total cloud cover and sea ice concentrations from 1976 to 2005 in September, October, and November. These linear trends were obtained with the least squares method. As shown in Fig. 3a and b, the negative trends in sea ice concentrations are found widely in the Laptev Sea, the East Siberian Sea and the Beaufort Sea in September. Additionally, in the Atlantic sector, the negative trends are seen in the Kara Sea and the Barents Sea. For the cloud cover, a significant trend is scarcely observed, limited to only the coast of the East Siberian Sea and northern Bering Strait.

Negative trends in sea ice concentration remain in October (Fig. 3b), although the area of significant negative trends becomes narrower than that in September. However, positive trends in cloud cover exist broadly over the Arctic Ocean. In the region of the East Siberian and Beaufort Sea, where the sea ice significantly decreases, larger positive trends in the cloud cover are found. Therefore, the increased cloud cover is confirmed to result from the reduction in sea ice. Note that the cloud cover increases significantly over the Arctic Ocean north of the Beaufort Sea, although significant negative trends in sea ice concentrations are not found.

In November, Fig. 3c shows that the significant negative trends in sea ice concentration are limited to the Barents Sea, the Bering Strait and the coasts of Greenland. Over these regions, a significant increase in cloud cover is found. This result also supports the model that the cloud cover increases because of reduced sea ice. In winter months, the cloud cover increases over grids with reduced sea ice, similar to that in November (not shown). However, because the sea ice reductions in November and winter months are smaller than that in October, the cloud cover change averaged over

ACPD
15, 17527–17552, 2015

the Arctic Ocean in these months is less significant than that in October. The following subsections focus on the increased cloud cover in October.

3.2 Cloud cover changes resulting from reduced sea ice

As shown in Fig. 3, the retreating Arctic sea ice in September and October is significant, but the positive trends in cloud cover in September are less than those in October. As the open ocean extends because of the reduced sea ice, vertical heat and moisture fluxes from the ocean to the atmosphere are enhanced. Figure 4 shows linear trends in the latent heat (LE) and sensible heat (SH) fluxes in September and October. Positive trends are exhibited in the LE and SH at grids, where sea ice reduced remarkably. The increase in both fluxes is larger in October than in September because of the large temperature difference between the atmosphere and the sea surface in October. Because the air temperature normally decreases from September to October along with the seasonal cycle, the difference between the air temperature and sea surface temperature is greater in October compared with that in September, causing the two fluxes to increase. The increase in the LE and SH fluxes can play a role in the increased cloud cover in October. These results are also consistent with previous studies (Blüthgen et al., 2012; Schweiger et al., 2008; Vavrus et al., 2011).

Figure 5 shows comparisons of the vertical profiles of the cloud fraction, relative humidity, air temperature and specific humidity in October between grids with and without significant reductions of sea ice. In this figure, the case "Δ ai−" is defined by grids with a linear trend of sea ice concentration less than $-0.1\,\mathrm{decade}^{-1}$. The case "Δ ai+" is defined by grids with linear trends of sea ice concentration of more than $0\,\mathrm{decade}^{-1}$. In the case Δ ai−, an increase in the cloud fraction is found in the lower troposphere centered at the $\sigma = 0.9$ level (approximately 830 m) (Fig. 5a and b). At the $\sigma = 0.9$ level, the cloud fraction increases by approximately 15 %. For the increase in the cloud fraction, the cloud liquid water grows through a large-scale condensation process, but the cloud ice shows little change. However, the cloud fraction decreases at levels below $\sigma = 0.95$. The cloud base height rises because of the reduced sea ice in the case

ACPD
15, 17527–17552, 2015

Δ ai− (not shown). Figure 5c and d shows that the relative humidity increases at levels between $\sigma = 0.9$ and $\sigma = 0.8$ (approximately 1839 m) for the case Δ ai−. This result is consistent with the increase in the cloud fraction. Decreases in the relative humidity are also found in levels below $\sigma = 0.9$, consistent with the decrease in the cloud fraction at levels below $\sigma = 0.95$ (approximately 460 m).

Figure 5e and f shows that the air temperature increases with the maximum increase at the surface. The significant increases in air temperature are found in layers between the surface and $\sigma = 0.85$ (approximately 1200 m) (Fig. 5f). Above $\sigma = 0.85$, the increases in the air temperature are smaller than in the underlying layers. Figure 5g and h shows that the specific humidity increases significantly in the lower troposphere. At the lowest level, the specific humidity increases by approximately 27 %. Compared with the change in the saturated specific humidity (qsat, dot-dot-dash lines in Fig. 5g and h), the increase in the specific humidity is near to that in the qsat at levels with increases in the cloud fraction. Therefore, the relative humidity increases and enhances the cloudiness in these levels (Fig. 5b and d). However, increases in the specific humidity are smaller than those in the qsat at thin layers near the surface. Therefore, in the surface thin layers, the relative humidity decreases and reduces the cloudiness.

Figure 6 shows the lapse rate of the air temperature and specific humidity. In the case Δ ai−, the lapse rate of the air temperature is large in the thin layers close to surface (Fig. 6a). Thus, the strong vertical diffusion effect of heat is confined in the surface thin layers. However, larger lapse rates are noted for the specific humidity between the surface and $\sigma = 0.8$ (Fig. 6b). The specific humidity is not limited to the surface thin layer, in contrast to the air temperature. Therefore, the vertical diffusion effect of moisture is enhanced in all levels of the lower troposphere. Hence, much more water vapor is transported from the ocean to higher atmospheric levels relative to the heat transferred. These effects cause different vertical profile changes in the air temperature and specific humidity.

The large lapse rate in the air temperature is limited to the surface thin layer because of the radiative cooling in all atmospheric levels. The air temperature is therefore

ACPD
15, 17527–17552, 2015

unlikely to increase significantly in the lower troposphere. The air temperature rises significantly only in the surface thin layer. However, because no stationary sink is noted for moisture similar to the radiative cooling in the atmosphere over the Arctic Ocean, the water vapor from the ocean increases in the lower troposphere.

In the case Δ ai+, the humidity and air temperature increase slightly in the lower troposphere because of global warming. Thus, the effect of global warming on the atmosphere, particularly in the boundary layer, appears in a region of the Arctic Ocean without a reduction in sea ice; however, the effect is small.

3.3 Cloud radiative effect

Cloud cover change affects the energy balance through the cloud radiative effect (CRE). During the autumn–winter–spring seasons in the Arctic region and because of the reduced or absent incoming shortwave radiation, the DLR by clouds may play an important role in the surface energy balance in the Arctic region. In addition, increasing the DLR because of increasing both the water vapor content and air temperature is an important factor contributing to the AA during global warming (Rinke et al., 2013). Here, we introduce an index defined by the ratio $((\Delta CRE/\Delta CS)_{SDLR})$ between the change in the CRE of the surface DLR ($\Delta\,CRE_{SDLR}$) and the change in the clear-sky surface DLR ($\Delta\,CS_{SDLR}$). Figure 7 shows the annual time series of the index, $(\Delta CRE/\Delta CS)_{SDLR}$. The index is averaged only for Δ ai− grids. The $\Delta\,CRE_{SDLR}$ is positive in grids in which the sea ice is reduced because the cloud cover increases as a result of reduced sea ice. Additionally, the $\Delta\,CS_{SDLR}$ is positive over the entire Arctic Ocean because of the increased air temperature and moisture. The indexes in Fig. 7 are approximately 0.4–0.6 during the fall, winter and early spring, varying little among the seasons. An increase in the cloud cover as a result of reduced sea ice enhances the surface DLR. The all-sky surface DLR increases by approximately 40–60 % compared to the clear-sky surface DLR change. Thus, the change in the CRE because of the reduced sea ice cannot be disregarded as a factor affecting the AA. This finding disagrees with Rinke et al. (2013). However, the index shown in Fig. 7 is different from the averaged value over the Arctic

ACPD
15, 17527–17552, 2015

Ocean. The averaged value is smaller in the winter and early spring because the area with a significant sea ice reduction is small during these seasons. However, the index is close to zero in the summer because of the minimal changes in Arctic cloud cover because of the reduced sea ice. This behavior implies that the CRE change in the surface DLR in the summer is less important than the albedo change resulting from the reduced sea ice.

4 Discussion

As shown in Fig. 3b, increases in the cloud cover are found in the Arctic Ocean near the North Pole, where the sea ice does not decrease significantly. Figure 8a shows the vertical profile of the cloud fraction averaged for the region (210–240° E, 75–83° N) indicated with a gray line in Fig. 8b. Compared with the cloud fraction for 1976–1985, the cloud fraction for 1996–2005 increases by approximately 20 % in the lower troposphere. The height at which the increase in the cloud fraction occurs is lower than that in the Δai− case shown in Fig. 5a. Figure 8b shows the linear trend of the sea level pressure (SLP), moisture flux at 925 hPa, and their convergence in October. A negative SLP trend is noted in the East Siberian Ocean in which the sea ice is reduced during the period. This change in SLP enhances the atmospheric moisture transported from the lower latitude to the North Pole. Then, the moisture flux converges in the region including the area covered by the gray lines. Accordingly, the cloud fraction in the region near the North Pole increases in the lower troposphere despite the absence of a significant reduction in sea ice.

During global warming, both the air temperature and humidity increase, complicating the changes in Arctic cloud cover. Therefore, considering future Arctic cloud cover changes, increases in both air temperature and humidity are crucial components in addition to the sea ice loss. With regard to the vertical profile of the cloud cover change, the level at which the air temperature and humidity increases under global warming conditions is important. Thus, the fine vertical resolution and boundary process in the

ACPD
15, 17527–17552, 2015

model may be a primary factor for improving the projections of the Arctic cloud cover change related to global warming and sea ice loss in the future.

Previous studies have argued for a role of changes in Arctic cloud in the AA. Significantly increased DLR because of cloud cover occurs in grids with significant reductions in sea ice, whereas select studies have noted a lower effect of the increase in cloud cover on the surface DLR. These discrepancies in the effects should be related to the uncertainties of dealing with clouds and cloud radiative forcing among models. The vertical profile of cloud cover change is also strongly connected with the changes in cloud radiative forcing. The uncertainties in the air temperature and humidity increases may be among the causes. Therefore, further investigations into the Arctic cloud cover change and on the feedback process related to clouds are needed.

With regard to the feedback between the sea ice and clouds, the effects of cloud cover on sea ice are also considerable. This study focused on the changes in Arctic cloud cover as a result of the reduced sea ice. However, we were unable to observe a significant effect of the increased cloud cover on the sea ice reduction in our statistical analysis of inter-seasonal variations using monthly mean data, despite the increased surface DLR resulting from the increased cloud cover.

In the future, if the sea ice retreats further not only in the summer but also in the autumn and spring, then the Arctic cloud cover could increase more and the effects of the cloud cover could become stronger than the current period. Thus, a further understanding and correct projection of the relationship between the sea ice and cloud cover is important in the analysis of future global and Arctic climate change.

5 Summary

This study investigated the Arctic cloud cover change resulting from the reduced sea ice in global warming simulated by MIROC5 to understand the effect of changes in the extent of Arctic sea ice on cloud cover.

ACPD
15, 17527–17552, 2015

A significant negative trend for the Arctic sea ice is found in the summer and autumn during 1976–2005, although small negative trends in the winter and spring are found in limited regions. The temporal trend of the Arctic cloud cover is positive in the autumn-spring, with a maximum in October. This study focused on the increases in the cloud fraction in October resulting from the reduced sea ice.

In grids with reduced sea ice concentrations (trends below -0.1 decade^{-1}), the cloud fraction in October increases at levels between $\sigma = 0.9$ and $\sigma = 0.7$. However, the cloud fraction in grids without a reduction in the sea ice is unlikely to change. Because of the reduced sea ice, a more extensive open ocean area increases the latent and sensible heat fluxes from the ocean to atmosphere. Along with the seasonal progression, atmospheric temperature cooling increases the temperature gradient between the air and sea surface in October. Therefore, the fluxes from the ocean to the atmosphere are enhanced in October rather than in September. This effect results in a greater increase in the cloud fraction in October than in September.

Significant warming is found at the surface thin layer because the longwave radiative cooling suppresses warming in the overlying layers. However, because no stationary sink is available for the moisture such as the radiative cooling process in the atmosphere, moistening occurs throughout the lower troposphere. Thus, the cloud fraction increases throughout the lower troposphere except near the surface thin layers, in which the cloud fraction drops. Further, the cloud cover increases in regions close to the North Pole, at which no significant reductions in sea ice occur because the lower-tropospheric circulation is varied in response to the reduced sea ice.

The change in the CRE as a result of the reduced sea ice in the surface DLR is approximately 40–60 % compared to a change in clear-sky surface DLR in grids with significant sea ice reduction from autumn to spring. Therefore, the change in CRE resulting from the reduced sea ice must be considered as a factor influencing the Arctic amplification.

ACPD
15, 17527–17552, 2015

This study analyzed data from only one climate model, MIROC5. Therefore, the sea ice–cloud cover relationship in multiple models and its contribution to the uncertainty of future climate change projections among models are suitable future research topics.

Acknowledgements. This study was supported by the GRENE Arctic Climate Change Research Project conducted by the Ministry of Education, Culture, Sports, Science and Technology of the Japanese Government. We thank Y. Komuro and T. Suzuki for providing the land fraction data of MIROC5 to enable the calculations of the Arctic sea ice area. The Earth Simulator at JAMSTEC was employed to perform the AOGCM simulations.

References

Blüthgen, J., Gerdes, R., and Werner, M.: Atmospheric response to the extreme Arctic sea ice conditions in 2007, Geophys. Res. Lett., 39, L02707, doi:10.1029/2011GL050486, 2012.

Comiso, J. C.: Warming trends in the Arctic from clear sky satellite observations, J. Climate, 16, 3498–3510, 2003.

Comiso, J. C., Parkinson, C. L., Gersten, R., and Stock, L.: Accelerated decline in the Arctic sea ice cover, Geophys. Res. Lett., 35, L01703, doi:10.1029/2007GL031972, 2008.

Curry, J. A., Schramm, J. L., and Ebert, E. E.: Sea ice-albedo climate feedback mechanism, J. Climate, 8, 240–247, 1995.

Dickinson, R., Meehl, G., and Washington, W.: Ice-albedo feedback in a CO_2-doubling simulation, Climatic Change, 10, 241–248, 1987.

Hahn, C. J., Warren, S. G., and London, J.: The effect of moonlight on observation of cloud cover at night, and application to cloud climatology, J. Climate, 8, 1429–1446, 1995.

Hansen, J., Ruedy, R., Sato, M., and Lo, K.: Global surface temperature change, Rev. Geophys., 48, RG4004, doi:10.1029/2010RG000345, 2010.

Hasumi, H.: CCSR Ocean Component Model (COCO), version 4.0, Center for Climate System Research Rep. 25, 103 pp., available at: http://ccsr.aori.u-tokyo.ac.jp/~hasumi/COCO/coco4.pdf (last access: 26 June 2015), 2007.

Holland, M. M. and Bitz, C. M.: Polar amplification of climate change in coupled models, Clim. Dynam., 21, 221–232, 2003.

Kay, J. E. and Gettelman, A.: Cloud influence on and response to seasonal Arctic sea ice loss, J. Geophys. Res.-Atmos., 114, D18204, doi:10.1029/2009JD011773, 2009.

ACPD
15, 17527–17552, 2015

Komuro, Y., Suzuki, T., Sakamoto, T. T., Hasumi, H., Ishii, M., Watanabe, M., Nozawa, T., Yokohata, T., Nishimura, T., Ogochi, K., Emori, S., and Kimoto, M.: Sea-ice in twentieth-century simulations by new MIROC coupled models: a comparison between models with high resolution and with ice thickness distribution, Journal of Meteorological Society of Japan, 90, 213–232, 2012.

Lean, J., Rottman, G., Harder, J., and Kopp, G.: SORCE contributions to new understanding of global change and solar variability, Sol. Phys., 230, 27–53, 2005.

Liu, Y., Key, J. R., Liu, Z., Wang, X., and Vavrus, S. J.: A cloudier Arctic expected with diminishing sea ice, Geophys. Res. Lett., 39, L05705, doi:10.1029/2012GL051251, 2012.

Manabe, S. and Stouffer, R. J.: Sensitivity of a global climate model to an increase of CO_2 concentration in the atmosphere, J. Geophys. Res.-Oceans, 85, 5529–5554, 1980.

Morice, C. P., Kennedy, J. J., Rayner, N. A., and Jones, P. D.: Quantifying uncertainties in global and regional temperature change using an ensemble of observational estimates: the HadCRUT4 data set, J. Geophys. Res.-Atmos., 117, D08101, doi:10.1029/2011JD017187, 2012.

Perovich, D. K., Light, B., Eicken, H., Jones, K. F., Runciman, K., and Nghiem, S. V.: Increasing solar heating of the Arctic Ocean and adjacent seas, 1979–2005: attribution and role in the ice-albedo feedback, Geophys. Res. Lett., 34, L19505, doi:10.1002/2014GL059356, 2007.

Porter, D. F., Cassano, J. J., and Serreze, M. C.: Local and large-scale atmospheric responses to reduced Arctic sea ice and ocean warming in the WRF model, J. Geophys. Res.-Atmos., 117, D11115, doi:10.1029/2011JD016969, 2012.

Rayner, N. A., Parker, D. E., Horton, E. B., Folland, C. K., Alexander, L. V., Rowell, D. P., Kent, E. C., and Kaplan, A.: Global analyses of sea surface temperature, sea ice, and night marine air temperature since the late nineteenth century, J. Geophys. Res.-Atmos., 108, 4407, doi:10.1029/2002JD002670, 2003.

Rinke, A., Dethloff, K., Dorn, W., Handorf, D., and Moore, J. C.: Simulated Arctic atmospheric feedbacks associated with late summer sea ice anomalies, J. Geophys. Res.-Atmos., 118, 7698–7714, 2013.

Sato, K., Inoue, J., Kodama, Y.-M., and Overland, J. E.: Impact of Arctic sea-ice retreat on the recent change in cloud-base height during autumn, Geophys. Res. Lett., 39, L10503, doi:10.1029/2012GL051850, 2012.

Sato, M., Hansen, J. E., McCormick, M. P., and Pollack, J. B.: Stratospheric aerosol optical depths, 1850–1990, J. Geophys. Res.-Atmos., 98, 22987–22994, 1993.

ACPD
15, 17527–17552, 2015

Schweiger, A. J.: Changes in seasonal cloud cover over the Arctic seas from satellite and surface observations, Geophys. Res. Lett., 31, L12207, doi:10.1029/2004GL020067, 2004.
Schweiger, A. J., Lindsay, R. W., Key, J. R., and Francis, J. A.: Arctic clouds in multiyear satellite data sets, Geophys. Res. Lett., 26, 1845–1848, 1999.
Schweiger, A. J., Lindsay, R. W., Vavrus, S., and Francis, J. A.: Relationships between Arctic Sea Ice and clouds during autumn, J. Climate, 21, 4799–4810, 2008.
Screen, J. A. and Simmonds, I.: Increasing fall-winter energy loss from the Arctic Ocean and its role in Arctic temperature amplification, Geophys. Res. Lett., 37, L16707, doi:10.1029/2010GL044136, 2010.
Serreze, M. C. and Barry, R. G.: Processes and impacts of Arctic amplification: a research synthesis, Global Planet. Change, 77, 85–96, 2011.
Smith, T. M., Reynolds, R. W., Peterson, T. C., and Lawrimore, J.: Improvements to NOAA's historical merged land–ocean surface temperature analysis (1880–2006), J. Climate, 21, 2283–2296, 2008.
Vavrus, S., Waliser, D., Schweiger, A., and Francis, J.: Simulations of 20th and 21st century Arctic cloud amount in the global climate models assessed in the IPCC AR4, Clim. Dynam., 33, 1099–1115, 2009.
Vavrus, S., Holland, M., and Bailey, D.: Changes in Arctic clouds during intervals of rapid sea ice loss, Clim. Dynam., 36, 1475–1489, 2011.
Wang, X. and Key, J. R.: Recent trends in Arctic surface, cloud, and radiation properties from space, Science, 299, 1725–1728, 2003.
Watanabe, M., Suzuki, T., O'ishi, R., Komuro, Y., Watanabe, S., Emori, S., Takemura, T., Chikira, M., Ogura, T., Sekiguchi, M., Takata, K., Yamazaki, D., Yokohata, T., Nozawa, T., Hasumi, H., Tatebe, H., and Kimoto, M.: Improved climate simulation by MIROC5: mean states, variability, and climate sensitivity, J. Climate, 23, 6312–6335, 2010.
Wu, D. L. and Lee, J. N.: Arctic low cloud changes as observed by MISR and CALIOP: implication for the enhanced autumnal warming and sea ice loss, J. Geophys. Res.-Atmos., 117, D07107, doi:10.1029/2011JD017050, 2012.
Yoshimori, M., Abe-Ouchi, A., Watanabe, M., Oka, A., and Ogura, T.: Robust seasonality of arctic warming processes in two different versions of the MIROC GCM, J. Climate, 27, 6358–6375, 2014.

ACPD
15, 17527–17552, 2015

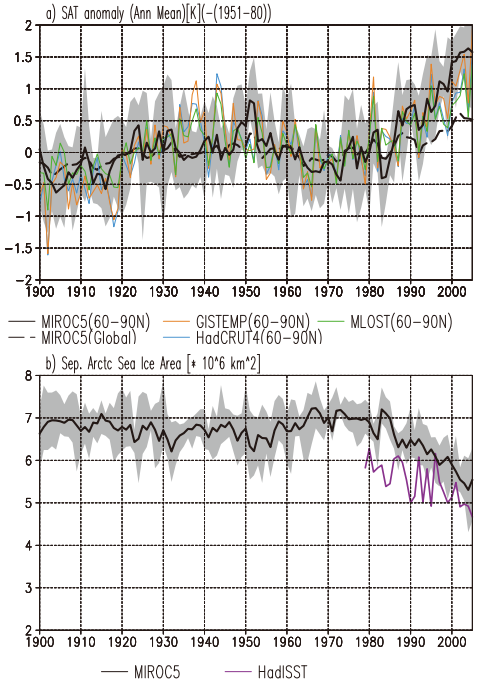

Figure 1. (a) Time series of the surface air temperature (SAT) anomaly from the 1951–1980 mean. Solid black, green, orange, and blue lines are the SAT anomalies averaged for the 60–90° N in MIROC5's ensemble mean, MLOST, GISTEMP, and HadCRUT4, respectively. The broken black line is the global and ensemble mean SAT anomaly in MIROC5. The gray shaded area indicates the maximum and minimum SAT anomalies between the ensemble members of MIROC5. **(b)** Time series of the September sea ice extent. The black lines are the ensemble mean. The gray shaded area indicates the maximum and minimum extent between the ensemble members. The purple line is the September sea ice extent calculated from HadISST. The units of the SAT anomaly and sea ice extent anomaly are K and 10^6 km^2, respectively.

ACPD
15, 17527–17552, 2015

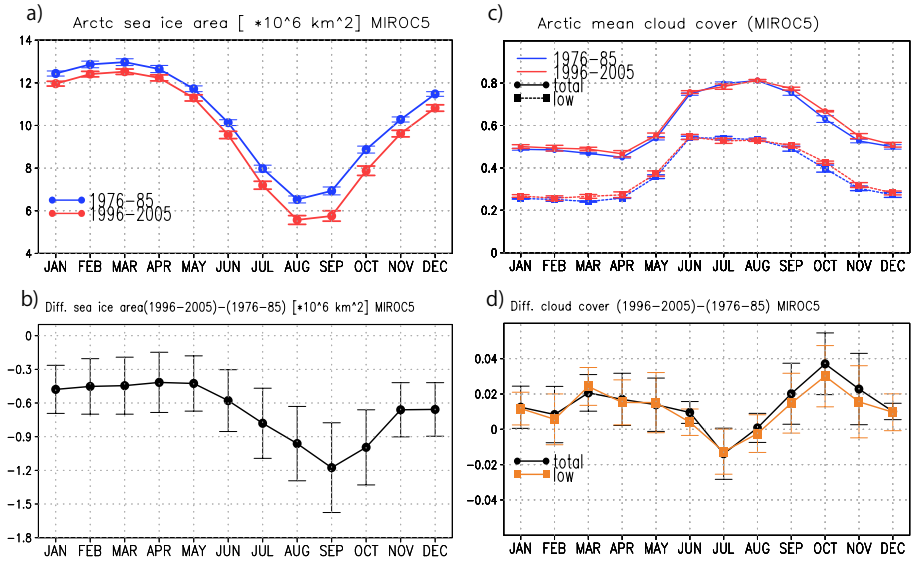

Figure 2. Seasonal cycle of **(a)** Arctic mean sea ice area averaged for 1976–1985 and 1996–2005 and **(b)** the difference between the means. **(c)** and **(d)** are identical to **(a)** and **(b)** except for the total and low cloud covers. The unit of the sea ice area is 10^6 km^2.

ACPD
15, 17527–17552, 2015

Effect of retreating sea ice on Arctic cloud cover

M. Abe et al.

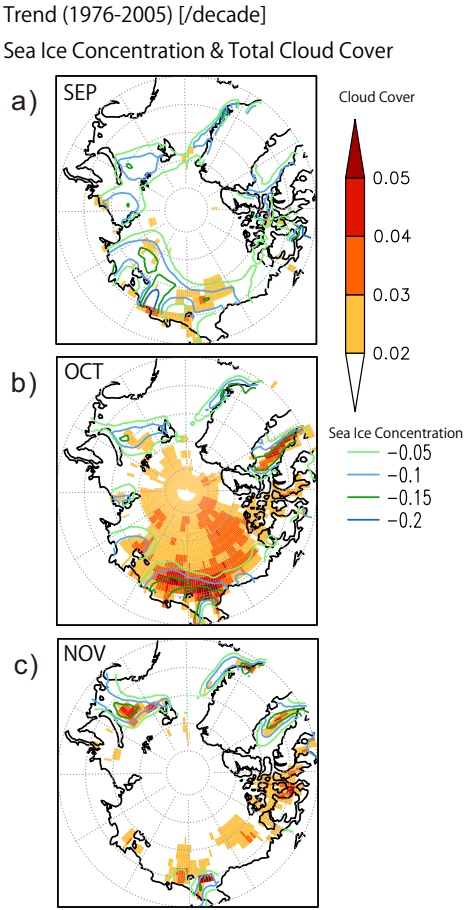

Figure 3. Geographical map of the linear trend in the total cloud cover (shade) and sea ice concentration (contour) in **(a)** September, **(b)** October, and **(c)** November during 1976–2005. The units are decade^{-1}.

ACPD
15, 17527–17552, 2015

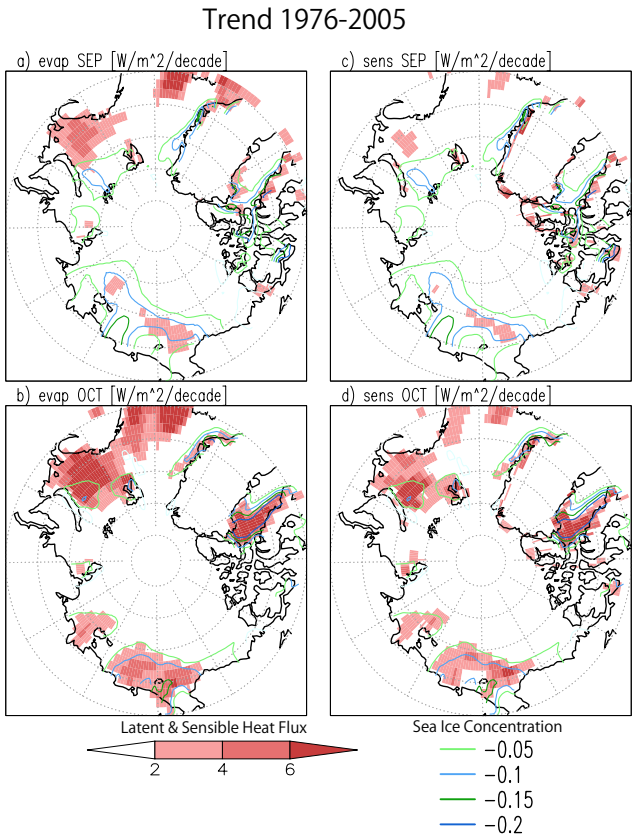

Figure 4. Geographical map of the linear trend in **(a, b)** the latent heat and **(c, d)** the sensible heat flux in **(a, c)** September and **(b, d)** October during 1976–2005. The units are $W m^{-2}$ decade^{-1}. A linear trend for the sea ice concentration (contour) is overlaid, and the units are decade^{-1}.

ACPD
15, 17527–17552, 2015

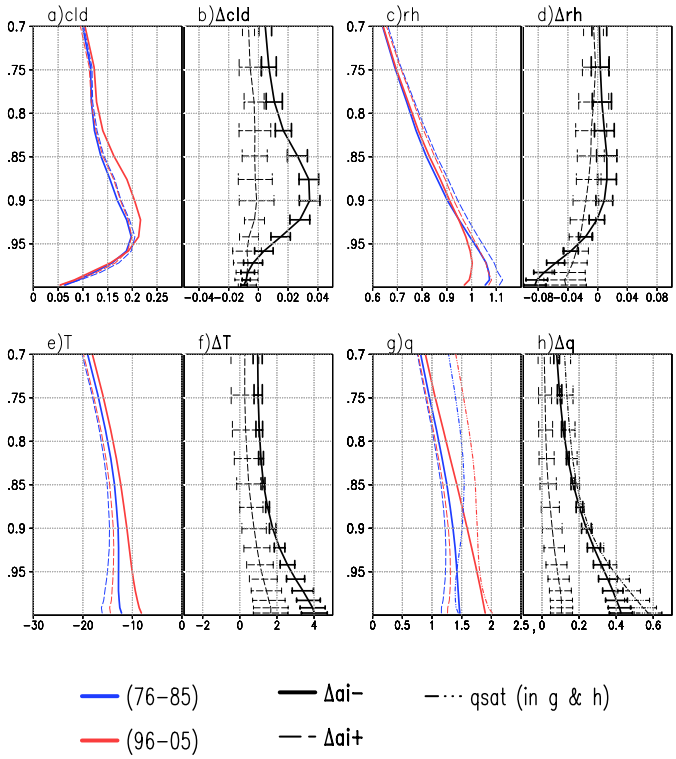

Figure 5. (a, c, e, g) Vertical profiles of the average for 1976–1985 (blue) and 1996–2005 (red) in the **(a)** cloud fraction, **(c)** relative humidity, **(e)** air temperature, and **(g)** specific humidity. The solid (broken) line represents the case Δ ai− (Δ ai+). See the text for the definition of the Δ ai− and Δ ai+. **(b, d, f, h)** Vertical profiles of the differences between the averages for 1976–1985 and for 1991–2005 in the **(b)** cloud fraction, **(d)** relative humidity, **(f)** air temperature, and **(h)** specific humidity. The solid (broken) line represents the case Δ ai− (Δ ai+). The dot-dot-dash lines in g and h indicate the saturated specific humidity. The units of the air temperature and specific humidity are K and g kg^{-1}, respectively.

ACPD
15, 17527–17552, 2015

Effect of retreating sea ice on Arctic cloud cover

M. Abe et al.

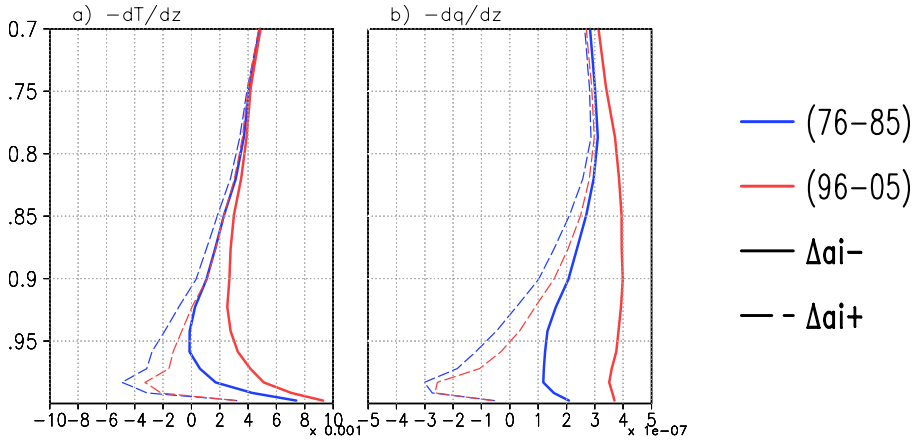

Figure 6. Vertical profiles of the lapse rate in the **(a)** air temperature and **(b)** specific humidity for 1976–1985 (blue) and 1996–2005 (red). The solid (broken) line represents the case Δ ai− (Δ ai+). The units of the lapse rate of the air temperature and the specific humidity are $\mathrm{K\,m^{-1}}$ and $\mathrm{g\,kg^{-1}\,m^{-1}}$, respectively.

ACPD
15, 17527–17552, 2015

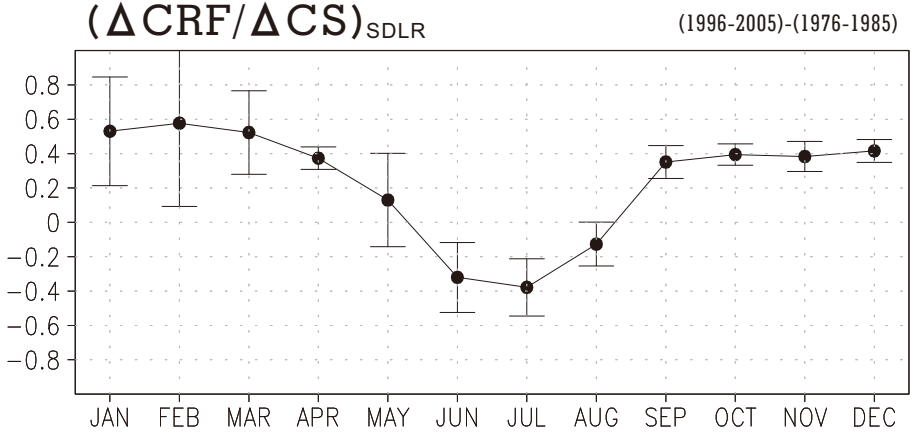

Figure 7. Annual time series of the index, $(\Delta CRE/\Delta CS)_{SDLR}$. See the text for the definition of the index. The indexes are for the case Δ ai−.

ACPD
15, 17527–17552, 2015

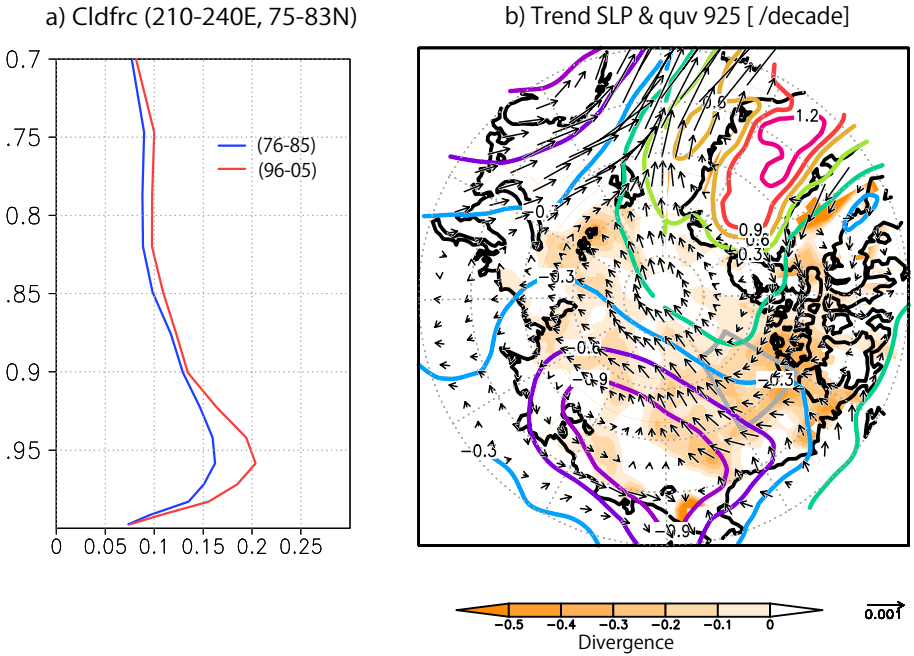

Figure 8. (a) Vertical profile of the cloud fraction for 1976–1985 (blue) and 1996–2005 (red) averaged in the region (210–240° E, 75–83° N) delineated by solid gray lines in **(b)**. **(b)** Linear trend of the sea level pressure (contour), moisture flux at 925 hPa (vector), and its convergence (shade). The unit of the moisture flux trend is (kg kg^{-1}) (m s^{-1}) decade^{-1}.

ACPD
15, 17527–17552, 2015